university of groningen

A Study on the Ball Check Valve.

How do operational parameters influence the behaviour of the ball check valve?

Femke Tas

S4254759

f.n.tas@student.rug.nl

Faculty of Science and Engineering

University of Groningen

The Netherlands

June 2023

XX

Abstract

In this thesis the behaviour of a ball check valve is studied with use of Comsol Multiphysics, a CFD software. A ball check valve is a valve that allows a fluid to flow in only one direction. Its main function is to prevent back flow, which can contaminate the fluid and cause malfunctioning of the system. The two forces that act on the body in the valve are the spring force and the drag force, whereas drag force consists of a pressure drag and a viscous drag. Multiple input parameters were varied to examine the effects on the behaviour of the valve. First the maximum in- and outlet pressure was enlarged which resulted in an earlier opening of the valve and a rise in viscous drag. The spring constant proved to have a proportional relation to the pressure whereat the valve opens. When the drag coefficient was calculated for these situations, it turned out that the values could not be compared with the literature value of the drag coefficient of a sphere. Hereafter the fluid type was altered from a Newtonian liquid to a non-Newtonian liquid and a gas. The inelastic models of the non-Newtonian liquid proved no substantial differences. Gas exerted a smaller viscous force on the sphere but reached a higher velocity than the liquid due to its lower viscosity and compressibility. The sphere was redesigned to a more aerodynamic droplet shape to study whether the drag force would decrease. However, not a significant reduce in drag was obtained as the shape was not completely streamlined. Finally, the closure of the valve was examined. There proved to be no back flow of the fluid during the closing, thus the fluid did not get contaminated.

Table of Contents

List of Figures

List of Tables

Nomenclature

Variables

γ	shear rate $[1/s]$
$\hat{\mathbf{i}}$	unit vector in the direction of free stream flow [-]
$\hat{\mathbf{n}}$	unit vector in the direction perpendicular to the body [-]
$\hat{\mathbf{t}}$	unit vector in the direction of shear stress [-]
μ	viscosity $[Pa \cdot s]$
ρ	density $[kg/m^3]$
A	cross-sectional area $[m^2]$
C_d	drag coefficient [-]
d	diameter $[m]$
F	force $[N]$
k	spring constant $[N/m]$
L	characteristic length of body $[m]$
p	pressure at body surface $[Pa]$
p_o	pressure far away of the body $[Pa]$
Q	flow rate $[m^3/s]$
Re	Reynolds number [-]
S	wet surface area $[m^2]$
T_w	shear stress acting on body surface $[N/m^2]$
v	velocity $[m/s]$
x	distance in vertical direction $[m]$

1 Introduction

A check valve or a non-return valve is a valve that allows a fluid to flow in only one direction. The check valves are fundamental for reliable pump operation. They must open and close quickly and easily and must provide a secure seal over a wide pressure range, as back flow can cause failures in a system. [4] A ball check valve plays a crucial role in improving sustainability in the automotive sector. It ensures reaching very high pressures by sending compressed fuel to the compression accumulator in an injection system in diesel and gasoline engines. The fuel injection system must be capable of performing multiple injections by carrying very high pressures, to facilitate different forms of advanced combustion to achieve low pollutant emissions. [5, 6]

In this thesis, COMSOL Multiphysics is used to simulate various scenarios within the ball check valve to gain understanding of dynamics and behaviour of the valve. This Computational Fluid Dynamics (CFD) software takes all principles of multiphysics into account and solves the Navier-Stokes Equations. The Navier-Stokes Equations dictate the motion of fluids and can be regarded as Newton's second law of motion for fluids. [7] Partial differential equations (PDE) describe the laws of physics for space- and time-dependent problems. Comsol utilises the Finite Element Method as a numerical method to compute approximations of the real solution to the PDE's. [8] To obtain reliable results the mesh will be analysed.

With the convenient mesh multiple parameters within the ball check valve will be modified. First the maximum in- and outlet pressure and spring constant will be varied to find a relation between these operational parameters and the opening time and pressure. With these variations also the drag force will be examined and the drag coefficient will be compared to the literature value of the body's drag coefficient. After this the fluid in the model will be adjusted from a Newtonian liquid to a gas and a non-Newtonian liquid. There will be a focus on what impact the fluid has on the drag force exerted on the ball and on the flow. Afterwards the shape of the ball will be redesigned to a more aerodynamic shape. It will be examined whether the behaviour of the check valve will differ when containing a different shaped body. Finally the closing of the valve will be considered. The importance is to observe how much time it takes for the valve to close and whether back flow is accompanied, and if so how much.

By varying multiple parameters this paper aims to answer the following research question:

How do operational parameters influence the behaviour of the ball check valve?

Figure 1: Ball check valve.

2 Theory

2.1 Ball Check Valve

In this section, the appearance (Figure 2) and operational mechanisms of the ball check valve, within the used system will be explained.

The ball check valve consists of a ball of steel resting in a nylon ring. A spring is attached to the ball to ensure that the ball is seated properly in the nylon o-ring. The ball is retained within the ball chamber. The ball is moved upwards when the pressure of the fluid below the ball surpasses the pressure above the ball. This allows the fluid to move through. Should the pressure beneath the ball be lower than above it, the ball would be compelled to return to rest in its original position in the nylon ring. A back flow accompanies the downward movement of the ball. Reducing back flow to the lowest possible level is critical, as back flow can cause failures in a system.

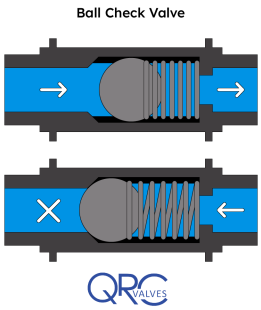

Figure 2: Cross section ball check valve adapted from [1].

2.2 Forces on the Ball

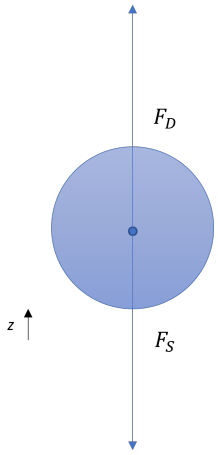

Figure 3: Forces acting on the ball.

In this model there are two forces acting on the ball in the z-direction. As can be established from Figure 3, the gravitational force is not taken into account in this model. The *spring force* results from the spring. The deformation of the spring creates a force in the opposite direction. The flow forces the ball in the positive z-direction and a force in the negative z-direction ensues. This restoring force causes the ball to return to its stable equilibrium position. This force is also known as Hooke's law. [9] As it is showed in equation 1 this law states that the force is directionally proportional to the displacement of the spring, x. k is a constant that is related to the kind of elastic material of the spring, and its shape and dimension.

$$F_s = -k \cdot x \tag{1}$$

A body moving in a fluid is subjected to drag force (Eq. 2). The force opposes motion, due to an object's shape, material and speed. [10]

$$F_D = \frac{1}{2}\rho v^2 C_d A \tag{2}$$

The drag is proportional to the fluids density, ρ, and to the square of the fluids velocity v. The area A is the frontal area, the body as seen from the stream, πr^2. In flow, past geometrically similar bodies with identical orientation and relative roughness, the drag coefficient C_d is a function of the Reynolds number. [11]

$$C_d = f(Re) \tag{3}$$

It varies with the free-stream velocity and viscosity and the characteristic length of the body, whereupon the Reynolds number is based.

$$Re = \frac{vL}{\mu} \tag{4}$$

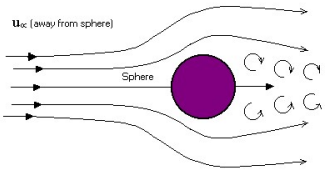

Figure 4: Drag force

The drag force consists of two components, which will be clarified now. Except at very low velocities, when the flow remains completely laminar, the wake directly downstream from the sphere becomes unstable. This leads to turbulent vortices which will be shed from various locations round the sphere. Due to turbulence, the pressure behind the sphere never fully recovers to match that on the upstream side and there will be a *pressure drag* to the downstream side of the sphere. (For purely laminar flow, the pressure recovery is complete, and the pressure drag is zero.) [12] This is added to the integrated shear stress of *friction drag*, which is also known as *viscous drag*, on the body. The sum of the two effects is known as the total drag force. In equation 5 is shown how the pressure coefficient and the viscous coefficient relate to the total drag coefficient. The integrals correspond to the drag forces exerted on the ball. Note that the pressure force depends on the pressure difference between the surface of the body and far away from the body, p - p_o. The viscous force rests on T_w, the magnitude of the shear stress on the body's surface dS. [13]

$$c_{\mathrm{d}} = \frac{2F_{\mathrm{d}}}{\rho v^2 A} = c_{\mathrm{p}} + c_{\mathrm{f}} = \underbrace{\frac{2}{\rho v^2 A}\int_S \mathrm{d}S(p - p_o)\left(\hat{\mathbf{n}}\cdot\hat{\mathbf{i}}\right)}_{c_{\mathrm{p}}} + \underbrace{\frac{2}{\rho v^2 A}\int_S \mathrm{d}S\left(\hat{\mathbf{t}}\cdot\hat{\mathbf{i}}\right)T_{\mathrm{w}}}_{c_{\mathrm{f}}} \tag{5}$$

Aerodynamic shaping can minimise the drag force. Streamlining will decrease the number and/or size of the turbulent vortexes. The pressure behind the object will be more similar to the pressure on the upstream side. This leads to a reduction of the pressure drag, hence the decrease of the drag force, which is now dominated by frictional drag.

For equation 2 to be valid, it is assumed that the body is immersed in a fluid with constant and uniform velocity field. The body must float in the free space. In the ball check valve model the body does not find itself in a free space with a uniform velocity field. The question that rises is whether equation 2 accounts for the situation in the valve.

2.3 Hypothesis

In the Introduction it is stated which input parameters are varied to analyse the behaviour of the ball check valve. A hypothesis is made on what those effects will be. When the maximum in- and outlet pressure of a fluid is increased, p - p_o (Eq. 5) will become larger, which will enlarge the pressure drag. The expectation is that the ball moves further upwards which gives a bigger flow of the fluid. When the spring constant is enlarged, the spring force will become larger (Eq. 1) and a greater drag force would be expected to let the ball ascend. When the fluid is adjusted to a more viscous fluid it is predicted that the shear stress on the body's surface is enlarged (Eq. 5) and thus the drag force will be increased, which will result in a larger ball displacement and a higher flow. Redesigning the shape to a more aerodynamic will cause less turbulent vortices and reduce the drag force. This will lead to a lower ball displacement and less flow of the fluid.

3 Model Description

3.1 Physical Model

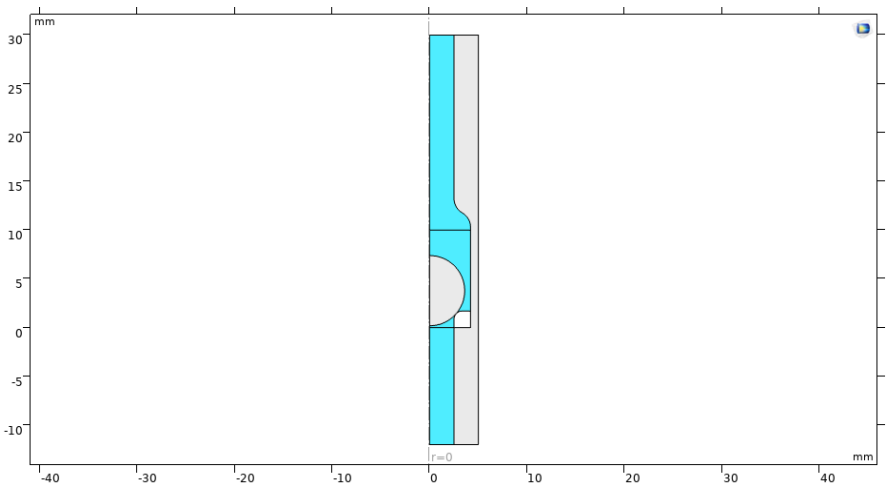

Figure 5: Comsol model ball check valve.

In Figure 5, the Comsol model of the ball check valve is depicted. For the purpose of the study, the geometry is reduced to a 2D axisymmetric cut. 3D models deliver extremely complex simulations. Reducing a 3D model to a simplified 2D model saves simulation time, without losing accuracy of the solutions. [14]

The valve consist of a structural steel pipe with a radius of 2.5 mm. The pipe broadens at the ball chamber, its radius is 4.2 mm. The sphere, made of structural steel, inside the ball chamber has a radius of 3.6 mm. In rest the ball is seated in the nylon o-ring. Since the system is defined to be isothermal, a constant temperature needs to be chosen. This is picked to be 293 Kelvin. The materials properties are shown in Table 1 below.

Table 1: Valve material properties.

Properties	Structural steel	Nylon
Density	7850 kg/m^3	1150 kg/m^3
Young's modulus	200 GPa	2 GPa
Poisson's ratio	0.3	0.4

The geometry does not include representation of the spring that keeps the ball against the O-ring; instead, a spring foundation is utilised. The spring constant is 4 N/m, and when the ball is at rest the spring is under 5 mm predeformation. [15] In order to maintain consistent initial conditions, the spring's predeformation is gradually increased using a smooth step function, depicted in Figure 6 below.

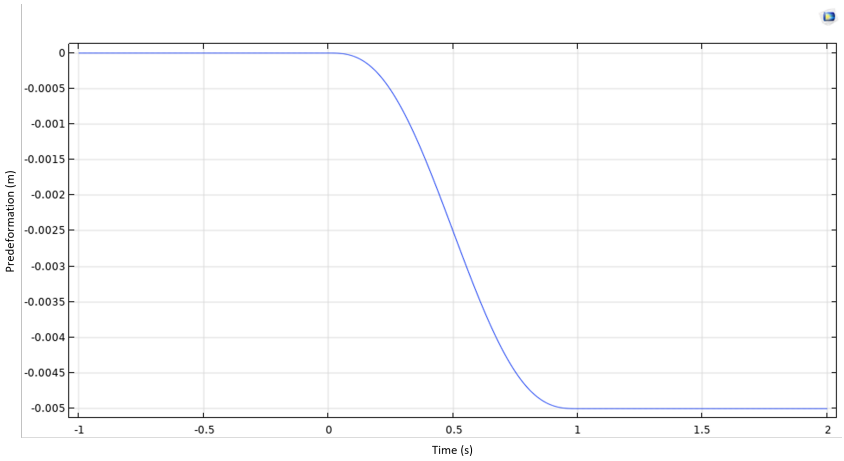

Figure 6: Ramp predeformation spring.

In the base model, water serves as a fluid. In other models the fluid type is varied to a gas or a non-Newtonian liquid. The material properties are shown in the Appendix in Table A.2. The maximum in- and outlet pressure in the original model is 2500 Pa. The inlet pressure gradually increases from 2 seconds as illustrated in Figure 7. The outlet pressure follows the plot in Figure 8. The maximum in- and outlet pressures will be varied between 1000 and 10000 Pa in different models. Finally, in the original model the body is shaped as a sphere. This shape will be compared to models with a droplet shaped body.

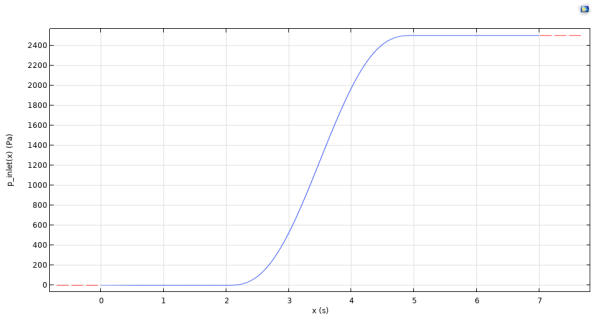

Figure 7: Ramp maximum inlet pressure.

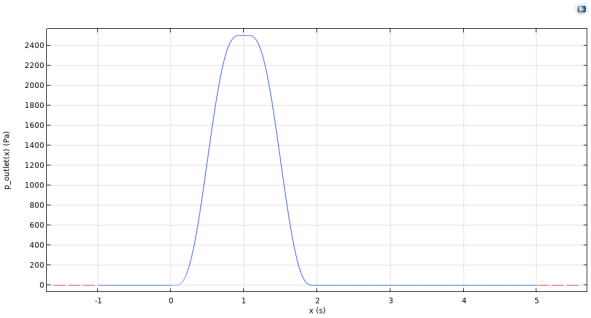

Figure 8: Maximum outlet pressure.

For the solid domains in this model Solid Mechanics are applied. The Navier-Stokes Equations are assigned to the turbulent fluid.

$$\underbrace{\rho\left(\frac{\partial \mathbf{v}}{\partial t}+(\mathbf{v}\cdot\nabla)\mathbf{v}\right)}_{\text{inertial forces}} = \underbrace{-\nabla p}_{\text{pressure forces}} + \underbrace{\nabla\cdot\left\{\mu\left[\nabla\mathbf{v}+(\nabla\mathbf{v})^{\mathrm{T}}-\tfrac{2}{3}(\nabla\cdot\mathbf{v})\mathbf{I}\right]\right\}}_{\text{viscous forces}} + \underbrace{\mathbf{F}}_{\text{external forces}} \tag{6}$$

The fluids density is characterised by ρ. v is the viscosity of the fluid. The p equals the fluids pressure and μ stands for the fluids dynamic viscosity. [16] The inertial forces explain Newtons second law in a moving system. The pressure forces and viscous forces present the drag force exerted on the ball. The spring force serves as the only external force, as the gravitational force is negligible in this model.

3.2 Mathematical Model

In this model the mesh is built with triangles and quadrilaterals. The solid parts consist of only triangles. This is different when it comes to the fluid. At the boundaries of the fluid, the mesh consists of quadrilaterals. The eight quadrilaterals decrease in size as the mesh reaches the boundary. The gradient of the velocity is at its highest there. More mathematical points are needed to describe the behaviour there, which explains the decrease in size.

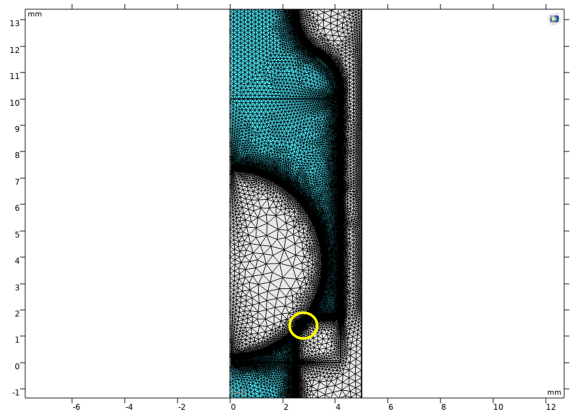

Figure 9: Mesh ball check valve.

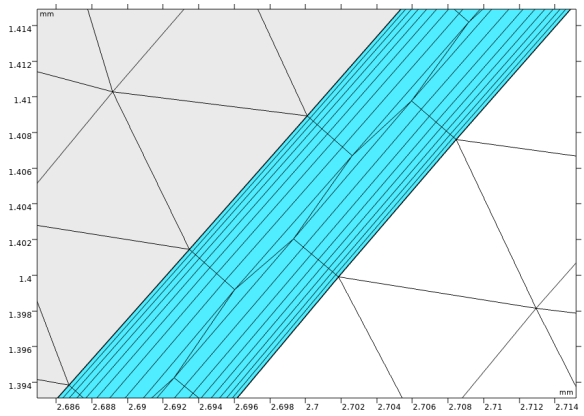

Figure 10: Mesh boundary layer fluid.

The mesh of the fluid is divided into three regions. The central fluid domain adopts a freely moving deformed mesh, whereas the bottom and top fluid domains make use of a fixed mesh. The central fluid domain also functions as the confinement of the displacement of the ball. The Arbitrary Lagrangian Eulerian (ALE) formulation applied for the discretization of the Navier-Stokes equations in a deforming domain requires that the topology of this domain does not adjust. In a real contact situation, the topology of the fluid domain changes as the parts get into contact. For a numerical analysis, an offset needs to be included in the contact settings to prevent the parts to physically touch each other. In this model, the offset is set to a very small value (5 μm) which is sufficient to preserve the fluid-domain topology while still preventing any significant flow in the reverse direction when the valve is closed. To obtain a satisfying accuracy of the solution, automatic remeshing is used when the ball is moving. In this model, the valve body is designed as rigid. This means that except for the contact region it could have been removed from the model completely. Keeping it will, however, allow better visualization of the model and results. [15]

3.3 Boundary and Initial Conditions

Boundary and initial conditions play a crucial role in mathematical and computational models to define the behaviour of a system at specific locations or at the beginning of a simulation. In this section the boundary and initial conditions of the ball check valve model are described.

Initial conditions specify the initial state of a simulation, from that point onwards the solution can evolve over time. In this model the following initial conditions are applicable:

- The fluids velocity is 0 m/s and the in- and outlet pressure is 0 Pa.
- The displacement of the ball is 0 m and its velocity is 0 m/s.
- The springs displacement is 0 m in the r-direction and in the z-direction the displacement follows the ramp function shown in Figure 6.

Boundary conditions describe literally the conditions on the boundary of a domain. They play an important role in determining the interaction between the system and its surroundings. The boundary conditions of this system are specified in the following manner:

- No slip condition applies for the fluids velocity at the boundaries.
- The displacement of the pipe is 0 m.
- The inlet and outlet pressure follow the plots in Figures 7 and 8.

4 Results and Analysis

4.1 Mesh Analysis

In the base model the mesh size is analysed. The model is run with eight different sizes, from extremely coarse to very fine. Parameters obtained from these simulations are shown in Table A.2 in the Appendix. The computation time (Table A.3 in Appendix) increases when decreasing the mesh size, as calculations are done at more points in the entire geometry. With the information collected from Table A.2 the reciprocal element size was plotted against the fluids flow rate, the viscous drag, the pressure drag and the total drag force, see Figure 11.

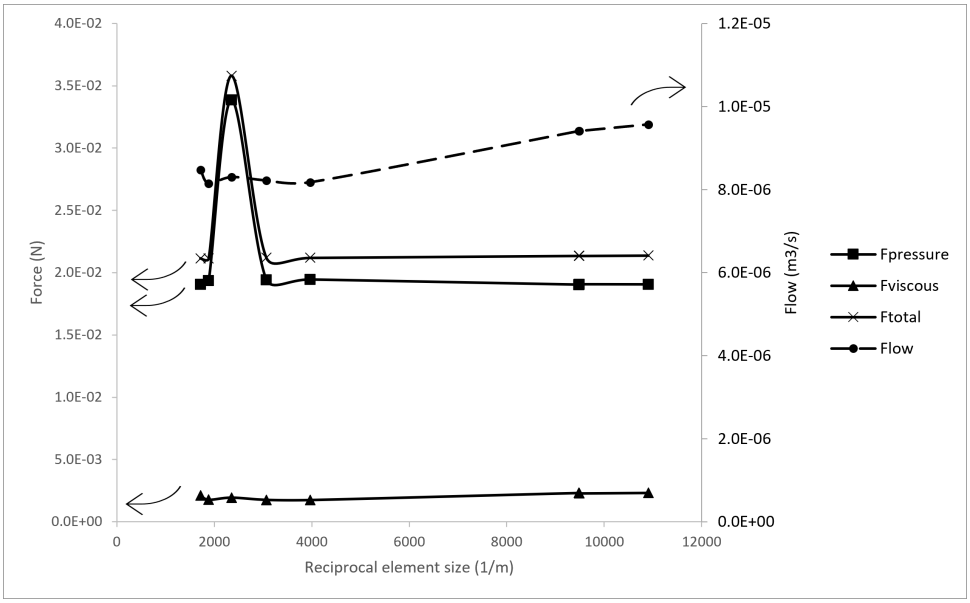

Figure 11: Reciprocal element size vs. flow.

From the figure it can be concluded that from a reciprocal element size of 9500 1/m reliable information is acquired as the curve flattens. Lower data presents some erratic behaviour and is therefore unreliable. Considering all curves, it results that all models should at least be run with the *Fine* element size.

4.2 Varying Maximum In- and Outlet Pressure and Spring Constant

In this section maximum in- and outlet pressures and spring constants are varied and the results are analysed. The pressures are in this particular range because at lower pressures the valve does not open and at higher pressures the body moves beyond the moving domain. For engineers it is crucial to know at what conditions the ball check valve will function. Thus the following parameters are used as input:

- Spring constant: 4 N/m and maximum in- and outlet pressure 1000 Pa - 2500 Pa.
- Spring constant: 20 N/m and maximum in- and outlet pressure 4500 Pa - 7000 Pa.
- Spring constant: 35 N/m and maximum in- and outlet pressure 8000 Pa - 10000 Pa.

It is important to know at which inlet pressure a check valve opens and when the opening takes place. With the operating curves obtained in Comsol (Appendix Figures A.1 - A.3) it can be derived at what inlet pressure a ball check valve opens with a particular spring constant. At this moment it is the first time that the drag force is bigger than the spring force. The spring force results from the 5 mm predeformation of the spring. In Table 2 it is presented at what time and exact pressure the check valve opens. In addition, the drag forces at that moment are included. These forces are obtained in Comsol by integrating the force acting on the ball over the total area of the ball.

Table 2: Opening of valve at different maximum inlet pressures and spring constants.

Spring constant	Spring force	Maximum inlet pressure (Pa)	Time (s)	Pressure (Pa)	$F_{d,p}$ (N)	$F_{d,v}$ (N)	F_d (N)	$F = P \cdot A$ (N)
4 N/m	0.02 N	1000	4.25	896.48	0.019902	0.000258	0.02016	0.01760
		1500	3.6629	901.49	0.019823	0.000224	0.020047	0.01770
		2000	3.4201	900.26	0.020017	0.000155	0.020172	0.01768
		2500	3.2734	901.28	0.020099	0.000133	0.020232	0.01770
20 N/m	0.1 N	4500	4.6	4413.5	0.09966	0.000709	0.10037	0.08666
		5000	4.2	4390.7	0.099602	0.000605	0.10021	0.08621
		5500	4.0175	4392.7	0.099553	0.000575	0.10013	0.08625
		6000	3.8902	4398.6	0.099525	0.000578	0.1001	0.08637
		6500	3.7908	4402	0.099547	0.000566	0.10011	0.08643
		7000	3.7092	4403.4	0.0996	0.000543	0.10014	0.08646
35 N/m	0.175 N	8000	4.4467	7626.7	0.17444	6.66E-04	0.17511	0.14975
		8500	4.25	7620.1	0.17464	4.79E-04	0.17512	0.14962
		9000	4.1281	7641.7	0.17446	6.66E-04	0.17512	0.15004
		9500	4.0299	7644.5	0.17452	6.39E-04	0.17516	0.15010
		10000	3.95	7648.3	0.17454	6.36E-04	0.17518	0.15017

With the use of Table 2 the relation between maximum inlet pressure, spring force and the opening time can be established. For each spring constant a certain pressure is needed to open the valve. When the spring constant is adjusted from 4 to 20 N/m the pressure to open the valve also increases with a factor 5. This proportional relation remains true when the spring constant is enlarged to 35 N/m. The time it takes to reach this opening pressure reduces with increasing maximum inlet pressure, as the pressures gradient is higher. The moment the valve opens, the drag force is higher than the spring force, which allows the body to move upwards. The drag force consists mainly of the pressure drag. The viscous drag is negligible as a limited amount of fluid has moved past the ball. In the last column of Table 2 the pressure force is calculated by multiplying the pressure to open the valve by the area of the pipe, which equals $\pi \cdot 0.0025^2 = 1.964 \cdot 10^{-5}$ m^2. The calculated pressure force is slightly smaller than the computed pressure drag. As the pressure is fixed, the area should be different than the area of the pipe. The ball is moving upwards so the vertical pressure force will cover an larger area. The computed pressure force is approximately 15 % larger than the calculated pressure force. This means that the area the vertical force acts on is 15 % larger as well, which equals $2.258 \cdot 10^{-5}$ m^2.

Table 3: Drag forces and coefficients at different inlet pressures and spring constants at t=5 s.

Spring constant	Maximum inlet pressure (Pa)	$F_{d,p}$ (N)	$F_{d,v}$ (N)	F_d (N)	Flow (m^3/s)	v (m/s)	$C_{d,p}$	$C_{d,v}$	C_d
4 N/m	1000	0.019812	5.21E-04	0.020333	8.87E-07	0.04517	477.8	12.6	490.4
	1500	0.019545	0.001308	0.020853	4.05E-06	0.206102	22.6	1.52	24.2
	2000	0.019393	0.00175	0.021143	6.77E-06	0.34462	8.04	0.73	8.77
	2500	0.019031	0.002324	0.021355	9.41E-06	0.47913	4.08	0.50	4.58
20 N/m	4500	0.099615	9.36E-04	0.10055	4.68E-07	0.023833	8630	81.1	8711.1
	5000	0.099205	0.001961	0.10117	1.69E-06	0.086102	658.5	13.0	671.5
	5500	0.098916	0.003006	0.10192	3.29E-06	0.167569	173.4	5.27	178.7
	6000	0.098928	0.003615	0.10254	4.79E-06	0.243993	81.8	2.99	84.8
	6500	0.099029	0.003868	0.1029	5.84E-06	0.297556	55.0	2.15	57.2
	7000	0.09898	0.004284	0.10326	7.03E-06	0.357887	38.0	1.65	39.7
35 N/m	8000	0.17432	0.00162	0.17594	7.70E-07	0.039207	218.8	2.03	220.8
	8500	0.17386	0.002658	0.17652	1.66E-06	0.084574	101.2	1.55	102.8
	9000	0.17344	0.003845	0.17728	2.83E-06	0.144268	59.2	1.31	60.5
	9500	0.17347	0.004442	0.17791	3.85E-06	0.196196	43.5	1.11	44.6
	10000	0.17349	0.005007	0.1785	4.88E-06	0.248485	34.4	0.99	35.4

At t=5 s the equilibrium situation has been reached as there is no displacement of the ball anymore. The spring force is equal to the drag force. With a constant spring constant, the drag force rises with the maximum inlet pressure. At a higher inlet pressure the spring attached to the ball is compressed further, resulting in a higher spring force and thus a higher drag force.

At this time the drag coefficients of the sphere are calculated with use of equation 2 to compare them to the literature value of the drag coefficient of a sphere in free space, which is 0.47 at Reynolds numbers between 10^4 and 10^6. [17] The drag forces and coefficients are depicted in Table 3. They differ enormously from the value taken from Hoerners book. The literature value is obtained from a model where the sphere is in free space, with a uniform velocity field and no pressure difference at the very beginning and end. This is absolutely different from the situation in the ball check valve model. The boundaries of the pipe wall prevent to let the fluid flow naturally, the walls force the fluid in a pattern which increases the velocity. This prohibits the existence of a uniform velocity field. Therefore the calculated drag coefficients can't be compared to the value from Hoerners book since the circumstances are not similar.

While the pressure drag remains close to constant, there is a pattern how the viscous forces evolve over maximum inlet pressure. With each spring constant the viscous force increases when a higher maximum inlet pressure is obtained. In Figure 12 the viscosity fields at t=5 s of 1000, 1500, 2000 and 2500 Pa are depicted. The size of the red part of the fluid, where it has the highest speed, gets bigger with higher inlet pressures. Because a larger part of the fluid that touches the ball has a higher velocity, the ball experiences more shear stress. This results in a higher viscous force exerted on the ball.

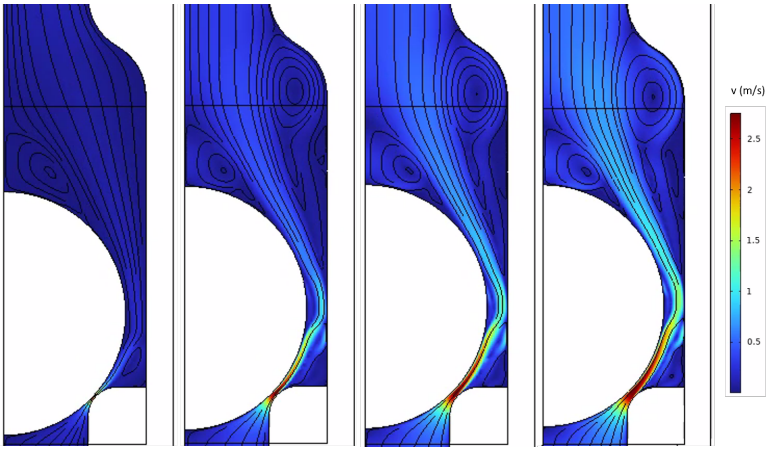

Figure 12: Velocity field at t=5 s, maximum inlet pressure L-R; 1000, 1500, 2000 and 2500 Pa.

4.3 Fluid Models

In this section the base model with water as fluid, a maximum in- and outlet pressure of 2500 Pa and a spring constant of 4 N/m, is compared to the model with a different fluid type. The comparing models will have hydrogen (gas) and blood (non-Newtonian liquid) as fluid.

In the models where the non-Newtonian fluid is applied, four inelastic models are analysed; Power Law, Bingham-Papanastasiou, Carreau and Casson-Papanastasiou. In Table A.4 in the Appendix the inserted parameters in the Comsol models, adapted from [18], are shown. In Figure 13 it is depicted per model how the viscosity of blood behaves compared to the shear rate. Blood is a shear thinning fluid as the viscosity lowers when the applied stress increases. The Power Law reacts abruptly when the applied shear rate is higher than its zero shear rate. The viscosity of the fluid in the other models reduces more gradually when a higher shear rate is applied. The zero shear viscosity differs among the four inelastic models (Table 4). A rheologic experiment in the laboratory would be needed to affirm which model corresponds best to the behaviour of blood.

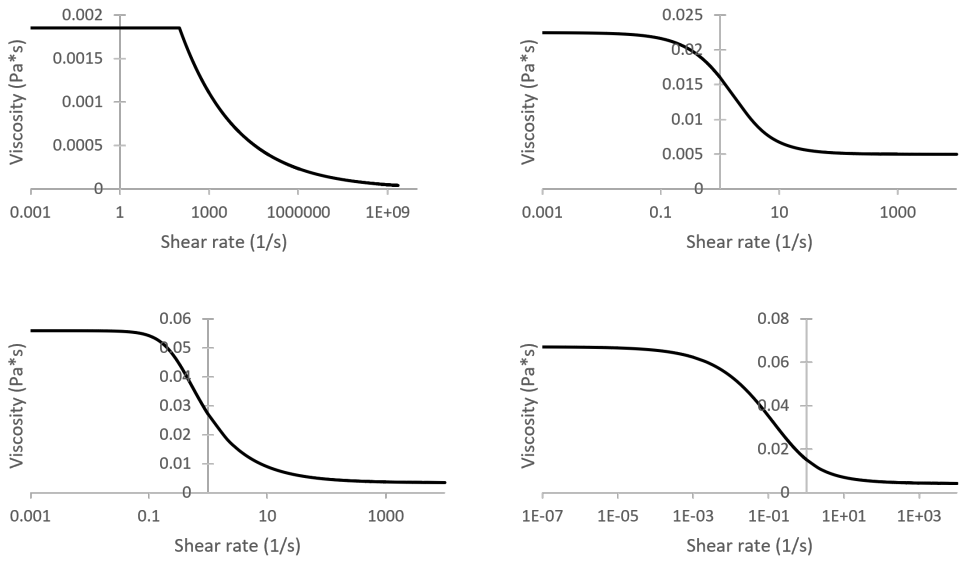

Figure 13: Shear rate vs. viscosity. L-R & top to bottom: Power Law; Bingham; Carreau; Casson.

Table 4: Forces on the ball with different fluid types.

	Zero shear viscosity (Pa·s)	$F_{d,p}$ (N)	$F_{d,v}$ (N)	F_d (N)	Flow (m^3/s)
Water	-	0.019031	0.002324	0.021355	9.41E-06
Hydrogen	-	0.02006	0.001662	0.021722	0.0013081
Power Law	0.001855	0.019725	0.001189	0.020914	7.16E-06
Bingham	0.0224	0.016889	0.005055	0.021944	1.16E-05
Casson	0.0672	0.017329	0.004404	0.021732	1.05E-05
Carreau	0.056	0.017725	0.003866	0.021591	9.89E-06

The drag forces that act on the solid sphere and the flow are computed in Comsol for each model. In Table 4 the computed values at the equilibrium position of the ball, at t=5 s, are presented. The flow of the fluid at t=5 s will be elaborated first. The flow of the Newtonian and non-Newtonian fluids is similar. With the increase of the inlet pressure, the flow of a fluid increases. The shear rate rises as result (Eq. 7). Typical for a shear thinning fluid as blood is that the rheologic behaviour looks more like water at higher shear rates. The flow of hydrogen is a factor 100 bigger than the flow of the liquids. Due to a lower viscosity (Table A.1), thus weaker intermolecular forces, the fluid endures less restrictions on molecular motion. This allows the molecules to move more freely at higher velocities. Also, as gases are compressible, their volume can be reduced under increased pressure, this facilitates rapid movement.

$$\dot{\gamma} = \frac{4Q}{\pi d^3} \tag{7}$$

The values of pressure drag and viscous drag variate per model. To find a reason behind these differences, the forces over the complete simulation time will be analysed. In Figure 14 - 16 the forces on the ball are plotted as a function of time. Until the valve opens, around 3.26 second, the forces exerted on the ball are equal. However, right after the opening of the valve the forces evolve differently per fluid and fluid model. The Bingham, Carreau and Casson model behave similarly, where the Bingham inelastic model obtains the most extreme values. The Power Law inelastic model follows a comparable path as water does, although the drag force that water exerts on the ball origins more from the pressure drag. The drag force that hydrogen exerts on the ball comes especially from the pressure drag. As a gas has a low viscosity it does not develop much shear stress when it touches the ball, so the viscous drag remains low.

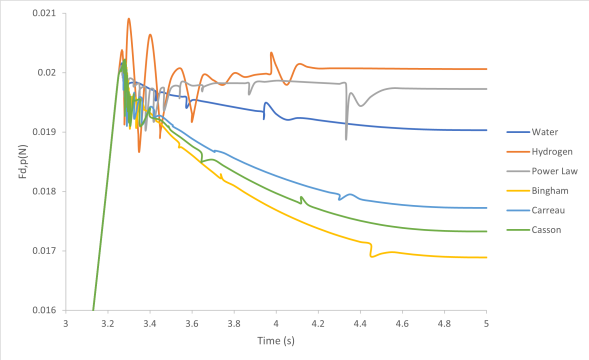

Figure 14: Pressure drag.

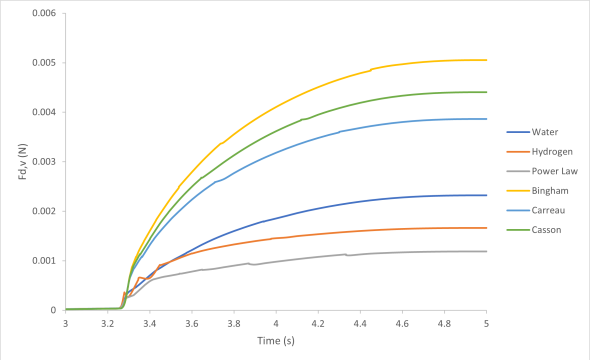

Figure 15: Viscous drag.

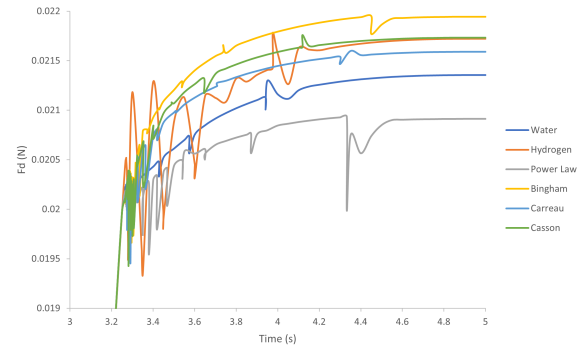

Figure 16: Drag force.

4.4 Shape of Ball

In this section the influence of the shape of the body on the behaviour of the ball check valve will be discussed. The new shape is created within the original model, with water as fluid, a maximum in- and outlet pressure of 2500 Pa and a spring constant of 4 N/m.

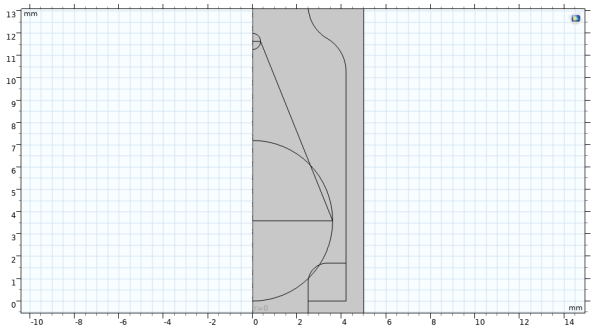

Figure 17: Geometry of streamlined shape.

The sphere is redesigned to a more aerodynamic droplet form. This shape should decrease the turbulent vortexes, which will reduce the pressure drag. 8.04 mm above the original spheres centre, a small sphere with r=0.36 mm is placed. Between the spheres a line is drawn to connect the spheres and create the advanced shape (Figure 17). The tail of the droplet is terminated with a sphere instead of a pointed cone as the mesh cannot calculate with a sharp pointed shape. The moving mesh domain is raised a bit as is visible in Figure 19.

Before zooming in on the forces exerted on the two bodies, the velocity and pressure field are interesting to evaluate when examining the influence of the shape of the ball on the performance of the ball check valve. In Figure 18 and 19 the velocity fields at t=5 s are projected. The velocity in the two models is comparable. The vortices, however, are not. The vortex directly behind the sphere is absent in the case of the droplet, due to more aerodynamic shaping. The vortex in the corner of the ball chamber remains to persist but is decreased in size.

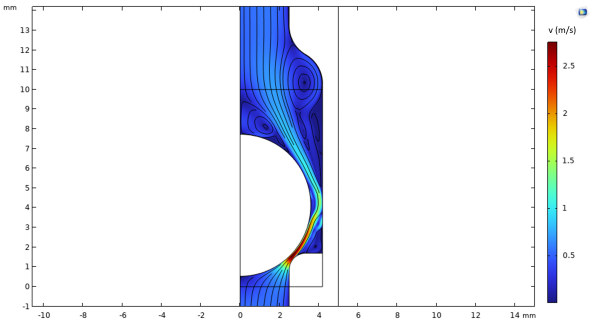

Figure 18: Velocity field sphere.

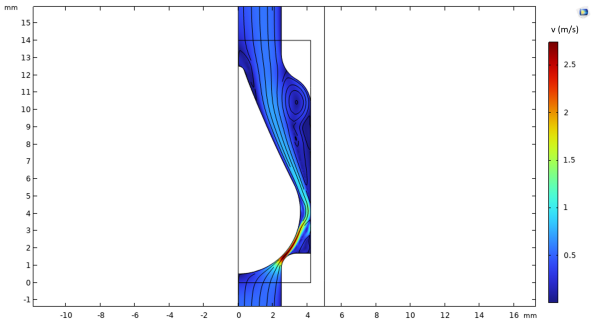

Figure 19: Velocity field droplet.

The positions of the vortices are clearly visible regarding the pressure fields in Figure 20 and 21. The darker blue spots above the bodies express the negative pressure at the location of the vortices.

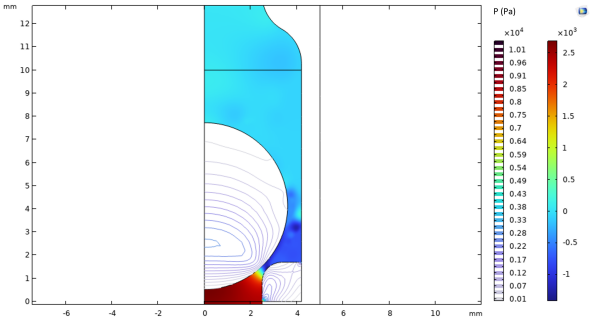

Figure 20: Pressure field sphere.

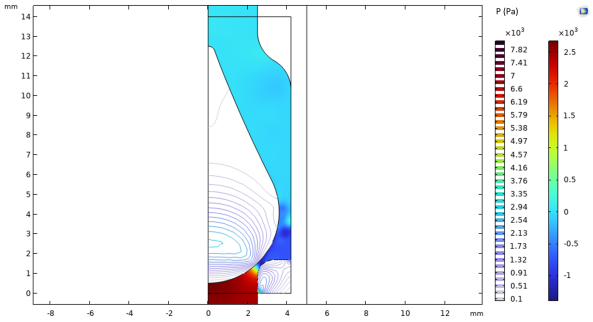

Figure 21: Pressure field droplet.

The drag forces, the flow and ball displacement of both shapes are noted in Table 5. These output parameters of the droplet shape are a slight bit smaller than the output parameters of the sphere. But in general it can be concluded that the differences in drag force, flow and ball displacement are minimal. The behaviour of the ball check valve with the droplet form is similar to the behaviour of the ball check valve containing the sphere. Fundamental differences would be visible if the redesigned shape would be completely streamlined. Unfortunately, this is impossible to achieve in this ball check valve with its boundary conditions and its condition that it can be closed.

Table 5: Output parameters droplet compared to sphere.

	Sphere	Droplet	Fraction droplet/sphere
$F_{d,p}$ (N)	0.019031	0.019003	0.998529
$F_{d,v}$ (N)	0.0023239	0.0022853	0.98339
F_d (N)	0.021355	0.021288	0.996863
Flow (m^3/s)	9.41E-06	8.91E-06	0.946841
Ball displacement (m)	3.39E-04	3.32E-04	0.980218

4.5 Closure of the Valve

In this final part of Results and Analysis the closing of the valve will be examined. In real life applications it is possible that due to complications the inlet pressure collapses suddenly. It is crucial for engineers to be aware of the consequences, for example the time it takes for the valve to close and how much back flow accompanies. Back flow can contaminate the fluid which can lead to malfunctioning of the system. Such a situation is modeled in this section.

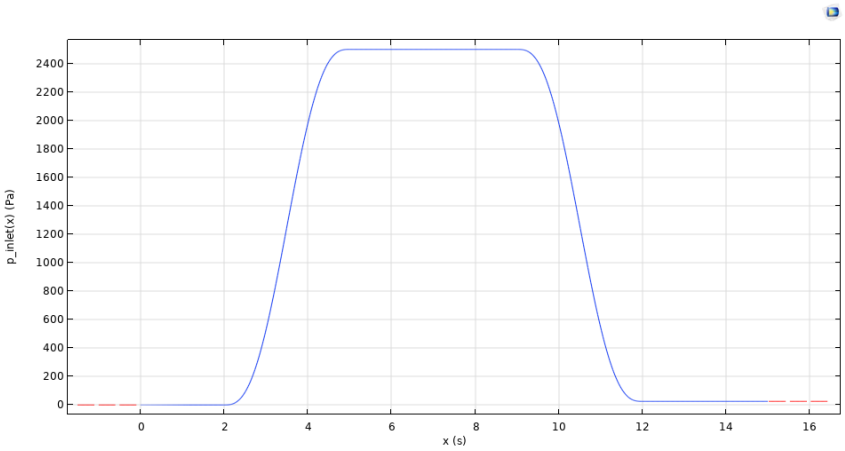

Figure 22: Inlet pressure as a function of time.

The original model is expanded to 15 seconds. The inlet pressure is kept constant from 5 to 9 seconds, after which it decreases until the pressure obtains a value of the maximum inlet pressure divided by 100, 25 Pa in this case (Figure 22). Initially an attempt to reach a final pressure of 0 Pa was done. An error occurred during the simulation, around 10.3 seconds, as the ball collided with the o-ring. Therefore the choice was made to reach a final pressure of the maximum inlet pressure divided by 100.

In Figure 23 is the ball displacement over the entire time scale depicted. The ball starts descending at 9.4 seconds and reaches the o-ring at 10.8 seconds. The profile of the inlet pressure differs slightly. The pressure starts decreasing 0.2 seconds earlier than the ball but reaches its final value at 12 seconds. This would mean that the ball would also be compelled to the o-ring at a smaller collapse of the inlet pressure.

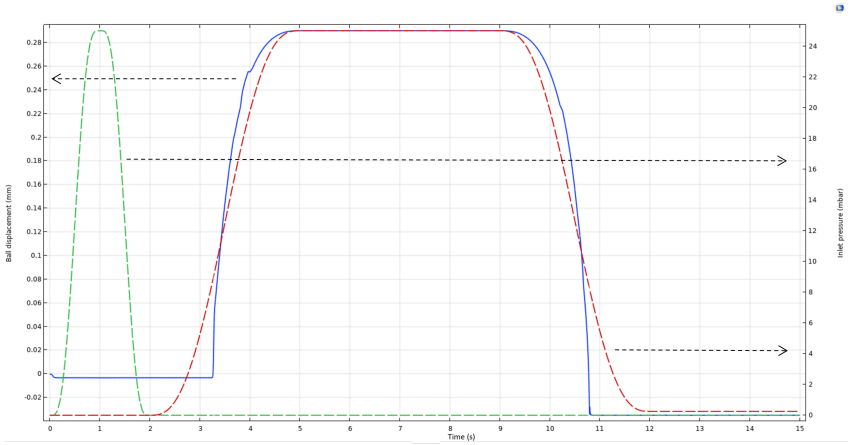

Figure 23: Ball displacement opening and closing of the valve.

There are a few moments where it is interesting to analyse how the velocity and pressure fields look like. These particular moments are listed and illustrated in Figure 24 and 25.

- At 3.26 s: the ball starts moving upwards.
- At 3.6 s: the ball is ascending quickly.
- At 5 s: the ball is floating at the same position.
- At 10.6 s: the ball is descending.
- At 10.8 s: the ball approaches the o-ring.
- At 15 s: the ball is resting in the o-ring.

In terms of elaboration on how the situation develops, it is important to consider the entire time frame. At 3.26 seconds, when the ball starts to ascend, the velocity of the flow is yet very small and the pressure behind the ball is close to zero as the flow has not passed in large amounts. At 3.6 seconds the ball is moving upwards due to the increasing pressure forces, resulting in a rise of the fluids velocity. Consequently the fluid does not stick to the ball anymore and a turbulent vortex occurs behind the ball. Directly after the gap between the body and the o-ring a negative pressure appears as the fluid is extracted there. This situation develops further to 5 seconds where a equilibrium position is reached. When the pressure starts declining the ball is to descend. First the velocity of the fluid will decrease as is depicted at 10.6 seconds and when the ball approaches the o-ring the fluid starts to flow backwards. The two vortices above the ball at 10.8 seconds occur because the fluid accumulates. The valve is completely closed at 15 seconds and a calm situation is attained.

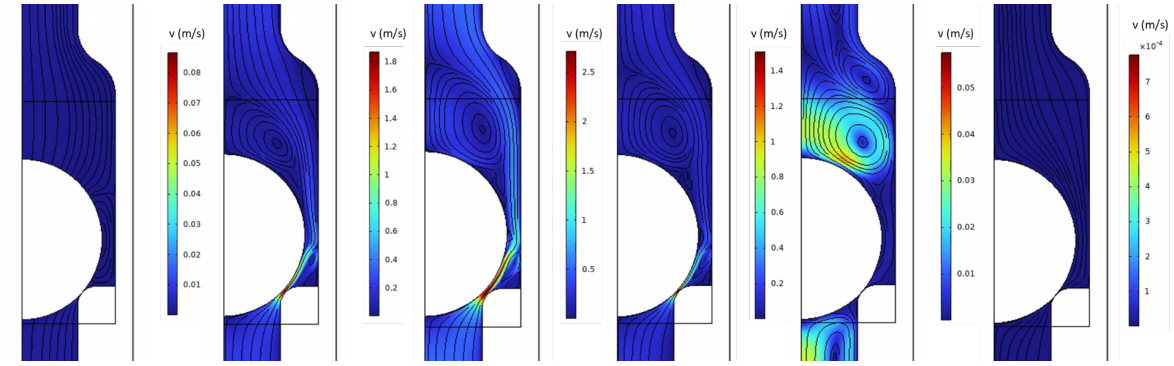

Figure 24: Velocity field; L-R at 3.26 s, 3.6 s, 5 s, 10.6 s, 10.8 s, 15 s.

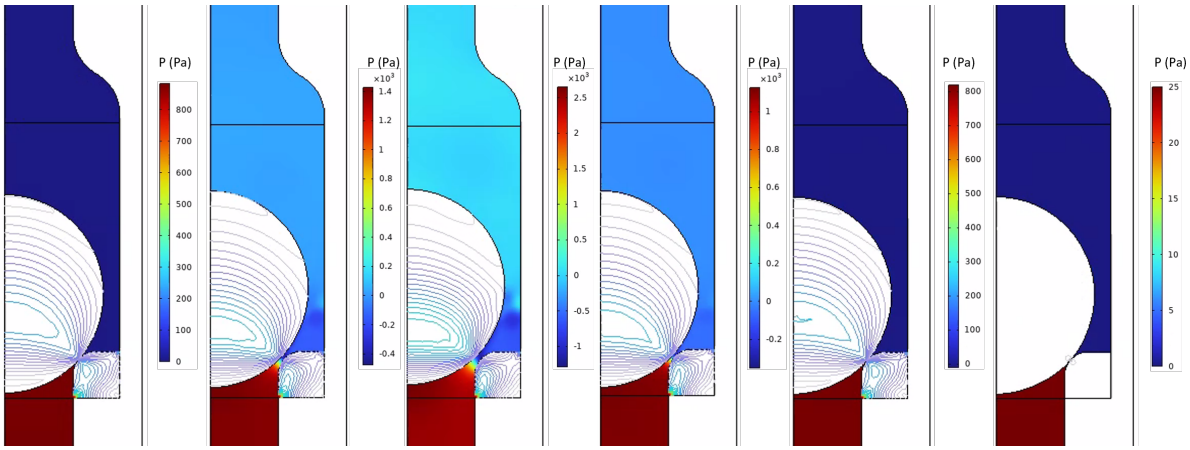

Figure 25: Pressure field; L-R at 3.26 s, 3.6 s, 5 s, 10.6 s, 10.8 s, 15 s.

It is of vital importance to know if and how much back flow accompanies the closing of the valve. In Figure 26 the flow over the complete time frame is plotted. The reduce in flow when the valve closes looks similar to the increase of the flow when the ball ascends. At 10.8 seconds the ball approaches the o-ring and erratic behaviour of the flow occurs. This happens because it approaches a situation where the ball and o-ring get into physical contact, which would be a highly non-linear problem. As surfaces get into contact, stress states will change abruptly. Solving such situations is incredibly challenging, which yields erratic behaviour. An equilibrium situation is reached around 12 seconds. The valve is closed, but there is still an offset between the ball and o-ring for numerical reasons. The flow has a positive value, even though 4.42 $\cdot 10^{-11}$ m^3/s is very small. A substantial negative flow does not occur during the closing of the valve. This means that the fluid does not get contaminated and there will be no malfunctioning of the valve due to contamination.

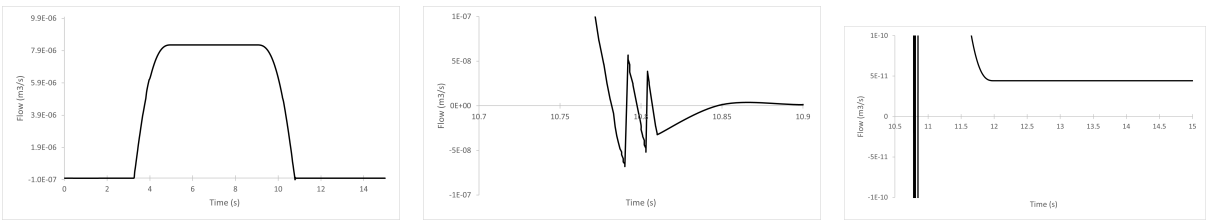

(a) Complete plot. (b) Erratic behaviour. (c) Flow when valve is closed.

Figure 26: Flow of opening and closure ball check valve.

5 Discussion

5.1 Feedback on hypothesis

In the hypothesis expectations about varying input parameters on the behaviour of the ball check valve were documented. In this section these expectations will be deliberated with use of the obtained results.

While the pressure force was expected to rise when higher inlet pressures would be applied, the viscous forces proved to increase. The area around the ball containing the maximum velocity expanded with increase of the pressure, what resulted in an increment of the shear stress on the ball. It is correct that the ball displacement and flow enlarges with high inlet pressures. Also the drag coefficient was calculated for each inlet pressure. These values could not be compared to the literature value of the drag coefficient as the body in the check valve does not float in free space with a constant and uniform velocity field.

When changing the fluid of the system the inelastic models showed diverse results. Experiments in the laboratory would declare which model suits the behaviour of a non-Newtonian liquid most accurately. Hydrogen did cause less viscous force as was expected, however the total drag force remained constant compared to water as fluid. The flow of gas was a factor 100 higher than the flow of liquid due to weak intermolecular forces en compressibility.

Redesigning the shape of the ball proved no significant difference. An entirely streamlined shaped would have functioned better to reduce the drag force. However, this was not attainable in the ball check valve because the radius of the lower part of the body could not be lowered due to the requirement of closing the valve. When the valve was closed within the original model it showed some erratic behaviour as the sphere and the o-ring came close to physical contact.

5.2 Improvements

To obtain more accurately and precise results the mesh can be refined, smaller time steps can be taken and the distortion when automatic remeshing occurs can be lowered. However, this would also result in longer computational times. A balance should be attained in the accuracy of the results and computational times.

5.3 Further recommendations

In this thesis a relatively general study on the behaviour of the ball check valve is conducted. Instead of varying multiple input parameters it would be interesting to focus on one component. More in-depth literature and computational research could be conducted on that specific focus point and the results could be correlated to research performed in the laboratory. For example, it could be interesting to study the effects of non-Newtonian fluids viscosity's in comparison to the viscosity of water by varying the inlet pressure.

6 Conclusion

This study on the ball check valve was conducted to research the effect of varying certain input parameters. With the use of Comsol Multiphysics, these scenarios were simulated. The mesh was proven to be accurate from a reciprocal element size of 9500 1/m and on wards. First the maximum in- and outlet pressure was raised and this enlarged the viscous drag, as the area of the maximum velocity increased. It was correctly predicted that the ball displacement and the flow rate increase with higher inlet pressures. The computed drag coefficients proved not to be comparable with the literature drag coefficient of a sphere as a uniform and constant velocity field of the sphere in free space is not applicable in this model of the ball check valve. When the spring constant was raised, this showed a proportional relation to the opening pressure of the valve.

Hereafter the fluid was changed to a non-Newtonian liquid. The four inelastic models did not show substantial difference to the behaviour of the valve with water as fluid. This is probably because blood is a shear thinning fluid and at higher shear stresses the rheologic behaviour matches that of water. When the fluid was changed to hydrogen the viscous drag reduced and the flow increased, due to its lower viscosity and its compressibility.

Following this, the sphere was redesigned to a droplet. This more aerodynamic shaping did not result in less drag force as was expected. Finally the closure of the valve was evaluated. The model shows some erratic behaviour around the closing time. There is no back flow when the check valve is closed, which prevents contamination of the fluid and malfunctioning of the entire system.

In conclusion, varying the pressure, spring constant and fluid type proved to influence the behaviour of the ball check valve. Redesigning the body did not effect the performance substantially.

7 References

[1] Ball Check Valves. URL https://qrcvalves.com/ball-check-valves/.

[2] The Engineering Toolbox. URL https://www.engineeringtoolbox.com/.

[3] Viscosity of Whole Blood. URL https://wiki.anton-paar.com/en/whole-blood/.

[4] John W. Dolan. Check Valve Problems. *LCGC North America*, 24(2), 2 2006.

[5] N D Petrea and C Bujoreanu. Importance of fuel injection system for low emissions, combustion noise and low fuel consumption. *IOP Conference Series: Materials Science and Engineering*, 444:042020, 11 2018. ISSN 1757-899X. doi: 10.1088/1757-899X/444/4/042020.

[6] Narcis-Daniel Petrea, Razvan-Constantin Iordache, and Carmen Bujoreanu. Analysis of Ball Check Valves with Conical and Spherical Seat Designs from Common-Rail Pumps. *Machines*, 10(10):959, 10 2022. ISSN 2075-1702. doi: 10.3390/machines10100959.

[7] Simon Schneiderbauer and Michael Krieger. What do the Navier–Stokes equations mean? *European Journal of Physics*, 35(1), 12 2014. ISSN 0143-0807. doi: 10.1088/0143-0807/35/1/015020.

[8] COMSOL. The Finite Element Method (FEM). URL https://www.comsol.com/multiphysics/finite-element-method?parent=physics-pdes-numerical-042-62.

[9] Adam Augustyn. Hooke's law. URL https://www.britannica.com/science/Hookes-law.

[10] Shane Maxemow. That's a Drag: The Effects of Drag Forces. *Undergraduate Journal of Mathematical Modeling: One + Two*, 2(1), 5 2013. ISSN 2326-3652. doi: 10.5038/2326-3652.2.1.4.

[11] Frank M. White. Fluid Mechanics. chapter 7.6. Mc Graw Hill, 9 edition.

[12] Drag Force on Solid Particles in Fluids, 9 2014. URL https://www.msubbu.in/ln/fm/Unit-IV/Drag.htm.

[13] Drag Coefficient. URL https://en.wikipedia.org/wiki/Drag_coefficient.

[14] Andrew Griesmer. Creating 2D Models from 3D Geometries in COMSOL Multiphysics, 5 2013.

[15] Comsol Multiphysics 6.0. Ball Check Valve. URL https://www.comsol.com/model/download/964121/models.sme.ball_check_valve.pdf.

[16] What Are the Navier-Stokes Equations?, 2015. URL https://www.comsol.com/multiphysics/navier-stokes-equations.

[17] Sighard F Hoerner. *Fluid-Dynamic Drag*. Hoerner, Sighard F, Bakersfield, CA, 1965.

[18] Aolin Chen, Adi Azriff Basri, Norzian Bin Ismail, and Kamarul Arifin Ahmad. The Numerical Analysis of Non-Newtonian Blood Flow in a Mechanical Heart Valve. *Processes*, 11(1):37, 12 2022. ISSN 2227-9717. doi: 10.3390/pr11010037.

8 Appendix

Table A.1: Fluid material properties. [2, 3]

Properties	Water (Newtonian fluid)	Blood (Non-Newtonian fluid)	Hydrogen (Gas)
Density	998.19 kg/m^3	1060 kg/m^3	0.0827 kg/m^3
Dynamic viscosity	1.0005E-3 Pa·s	2.87E-3 Pa·s	0.88E-5 Pa·s

Table A.2: Mesh analysis

	# of elements	Element size (m)	Reciprocal element size (1/m)	Fpressure (N)	Fviscous (N)	Ftotal (N)	Flow (m^3/s)	v (m/s)	$C_{d,p}$	$C_{d,v}$	C_d
Extremely coarse	3391	5.82E-04	1716.9	0.019044	0.002117	0.021162	8.47E-06	0.43135	5.036856	0.560021	5.597036
Extra coarse	4645	5.30E-04	1885.8	0.019365	0.001777	0.021142	8.15E-06	0.415107	5.530437	0.507521	6.037929
Coarser	8502	4.25E-04	2353.6	0.033862	0.00195	0.035812	8.3E-06	0.422667	9.327792	0.537184	9.864948
Coarse	11387	3.26E-04	3071.3	0.01943	0.001769	0.021199	8.22E-06	0.418555	5.457941	0.496777	5.954858
Normal	11527	2.52E-04	3971.7	0.019441	0.001756	0.021197	8.18E-06	0.41636	5.51878	0.498481	6.017261
Fine	80033	1.05E-04	9482.3	0.019031	0.002324	0.021355	9.41E-06	0.479128	4.079631	0.498169	4.577821
Finer	83381	1.05E-04	9488.6	0.019059	0.00229	0.021349	9.41E-06	0.479128	4.085633	0.49088	4.576535
Extra fine	94219	9.17E-05	10905.8	0.019051	0.002328	0.02138	9.57E-06	0.48728	3.948414	0.482531	4.431111

Table A.3: Computation time simulations. With the use of Lenovo YOGA C740, CORE i5.

Mesh size	Computation time	Remarks
Extremely coarse	26 min 5 sec	
Extra coarse	24 min 55 sec	
Coarser	29 min 44 sec	
Coarse	32 min 39 sec	
Normal	37 min 56 sec	
Fine	3 hours 11 min	200 iterations instead of 20
Finer	2 hours 44 min	
Extra fine	3 hours 26 min	

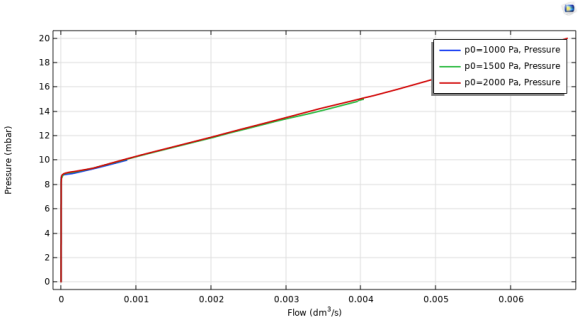

Figure A. 1: Operating curve; spring constant = 4 N/m.

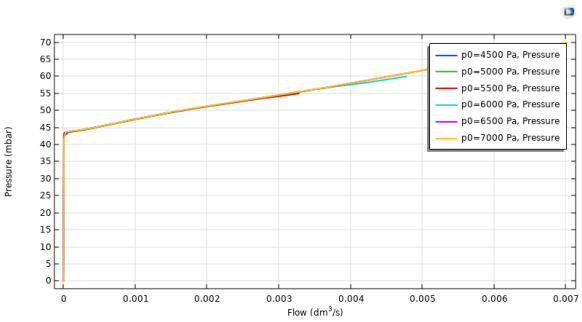

Figure A. 2: Operating curve; spring constant = 20 N/m.

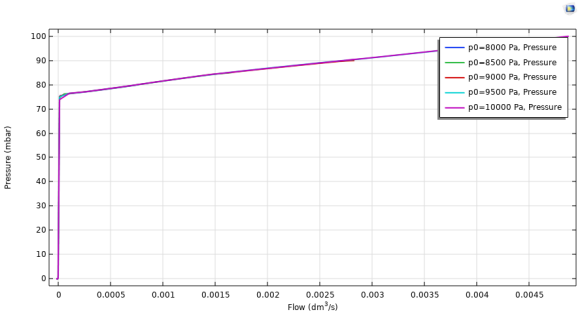

Figure A. 3: Operating curve; spring constant = 35 N/m.

Table A.4: Input parameters non-Newtonian models.

Power Law	Bingham-Papanastasiou	Carreau	Casson-Papanastasiou
Fluid consistency coefficient = 0.01467 Pa·s	Plastic viscosity = 0.0049721 Pa·s	Zero shear rate viscosity = 0.056 Pa·s	Plastic viscosity = 0.00414 Pa·s
Flow behaviour index = 0.7755	Yield stress = 0.0175 N/mˆ2	Infinite shear rate viscosity = 0.0035 Pa·s	Yield stress = 0.0038 N/m^2
Lower shear rate limit = 100 1/s	Model parameter = 1	Relaxation time = 3.313005 s	Model parameter = 10 s
Reference shear rate = 0.01 1/s		Power index = 0.3568	